Cataluminescence and Catalysis Properties of CO Oxidation Over Porous Network of ZrO_2 Nanorods Synthesized by a Bio-Template

Fei Teng[*,1,3], Yongfa Zhu[2], Gang He[3], Guizhi Gao[3] and Dennis Desheng Meng[*,1]

[1]*Department of Mechanical Engineering-Engineering Mechanics, Michigan Technological University, Houghton, Michigan 49931, USA*

[2]*Department of Chemistry, Tsinghua University, Beijing 10086, P.R. China*

[3]*School of Environmental Science and Engineering, Nanjing University of Information Science & Technology, Nanjing 210044, P.R. China*

Abstract: A network of ZrO_2 nanorods was prepared using the porous biomembranes as templates. The sample was characterized by SEM, XRD and nitrogen physicosorption isotherm. ZrO_2 nanoparticles were also prepared with a hydrothermal method in order to compare with this network. The results showed that after being calcined at 800 ^oC for 24 h, a volume contraction of ZrO_2 nanorod network occurred accompanied by a phase transformation of tetragonal-to-monoclinic ZrO_2; but the nanoparticles have grown into the large microparticles; as a result, ZrO_2 nanorod network has a higher BET area (45.7 m^2 g^{-1}) and a larger pore volume (0.20 cm^3 g^{-1}). The calcined network showed a higher cataluminescence (CL) intensity of CO oxidation and a higher combustion activity than the calcined particles, which was ascribed its high surface area, as well as advanced pores.

Keywords: ZrO_2 network, Biomembrane, CO, Cataluminescence, CH_4 combustion.

1. INTRODUCTION

Over the past few years, much research attention has been paid to one-dimensional nanostructures because of their potential applications in nanodevices [1-3]. It is well known that the properties of materials can be influenced by their physico-chemical structures. Recently, Y. Li *et al.* have reported that CeO_2 nanorods had a higher activity for CO oxidation than the nanoparticles. They attributed to the well-defined reactive crystal plane for single crystalline CeO_2 nanorods [4]. It is important for us to research the correlation of the morphology with properties of materials.

ZrO_2 has high strength and fracture toughness, high melting point, low thermal conductivity, and high corrosion resistance. ZrO_2 has been widely applied as structural materials, thermal barriers coatings, gas-sensing, solid oxide fuel cell, and catalysts [5-8]. A variety of anisotropic ZrO_2 particles, e.g., nanotubes [9-15], nanorods [16-18] and nano-laminae [19], have been researched. Compared with artificial templates, biological templates are generally cheap, abundant, and environmentally benign [20]. A variety of natural biological templates have been employed for the synthesis of porous materials with sophisticated structural ordering analogous to natural materials [21-28]. For example, Qi *et al.* reported a novel synthesis of ZrO_2 tubes [10] and hierarchically ordered macroporous networks composed of TiO_2 tubes [28] by using eggshell membranes as templates; but they did not show the physicochemistry properties of the tube network. Recently, biological templates, such as cuttlebone and inorganic skeletal plates of echinoids [22,23], organized bacterial threads [24, 25] and wood cellular structures [26,27], have been used to synthesize hierarchically ordered macroporous materials with bimodal porosity, which combined the good mass transport and accessibility of macroporous networks with the high surface area, selectivity, and catalytic properties of the smaller pore systems.

Following the report by Qi *et al.* [10], ZrO_2 nanorod network was prepared using eggshell membranes as templates while using inexpensive inorganic salts as precursors. The samples were characterized by SEM, XRD and N_2 adsorption isotherm. In this work, we have not obtained a network of ZrO_2 tubes. Moreover, CL properties of CO oxidation and combustion activity of CH_4 over the network of ZrO_2 nanorods were mainly researched. By comparison, ZrO_2 nanoparticles were also prepared by a hydrothermal method.

2. EXPERIMENTAL

Chemicals: The zirconium precursor, $ZrOCl_2$ was purchased from Beijing Chemical Company, Ltd.. Commercial eggs were locally available. All the other chemicals used in the experiments were of analytical grade and the water used was deionized.

2.1. Separation and Purification of Eggshell Membranes

Eggshell membranes can be easily isolated from eggshells. Briefly, eggs were gently broken and emptied the liquid egg white; then the manually separated membranes was washed with 1 M HCl solution to dissolve $CaCO_3$ and washed with water and ethanol thoroughly. Finally, the membrane was used as the template for the ZrO_2 coating.

*Address correspondence to these authors at the Department of Mechanical Engineering-Engineering Mechanics, Michigan Technological University, Houghton, Michigan 49931, USA; Tel: (+1) 906-487-3551;
E-mails: dmeng@mtu.edu, tfwd@hotmail.com

1876-214X/09

2.2. Synthesis of ZrO_2 Nanorod Network and Nanoparticles

The synthesis of ZrO_2 nanorod network follows the report by Qi *et al*. [10]. In a typical synthesis, the egg membrane was impregnated with a 0.25 M solution of $ZrOCl_2$ for 24 h under stirring. The template was taken out and then washed with deionized water to remove the remainder solution on template surface. The obtained sample was impregnated with a 2 M $NH_3 \cdot H_2O$ solution for 2 h and aged for 24 h. The sample was washed with water until no Cl ions can be detected by $AgNO_3$ solution. The resulting hybrid sample was dried at 80 ^oC overnight, calcined at 250 ^oC for 2 h and then 550 ^oC for 5 h in air to remove the bio-template.

To prepare ZrO_2 nanoparticles, 20 mL of 0.5 M $ZrOCl_2$ solution was mixed with 20 mL of 5 M NaOH solution under vigorous stirring for 0.5 h. The resulting colloid was put into a 50-mL autoclave and then subjected to hydrothermal treatment at 240 ^oC for 24 h. After cooling to room temperature, the solids were separated by centrifuging, washed with deionized water, and dried at 110 ^oC for 24 h.

To investigate the thermal stabilities of the samples, the samples were calcined at 800 ^oC for 24 h under flowing air.

2.3. Characterization

The morphology of the sample was characterized using SEM (KYKY 2800). The acceleration voltage was 15 keV and the current was 1.2 nA. The samples were characterized by X-ray diffraction (XRD) on a Rigaku D/MAX-RB X-ray powder diffractometer, using graphite monochromatized Cu Ka radiation (λ= 0.154 nm), operating at 40 kV and 50 mA. The patterns were scanned from 20º to 70º (2θ) at a scanning rate of 5º min^{-1}. A nitrogen adsorption isotherm was performed at 77 K on a Micromeritics ASAP2010 gas adsorption analyzer. Each sample was degassed at 200 ºC for 5 h before the measurement. Surface area and pore size distribution were calculated by BET (Brunauer-Emmett-Teller) and BJH (Barrett-Joyner-Halenda) methods, respectively.

2.4. Evaluation of Cataluminescence (CL) Properties

The CL detection system employed in this work consists of a CL-based sensor, a digital programmable temperature controller of the sensor, and an optical detector. The CL sensor was made by sintering a 0.2-mm-thick layer of the catalyst powder on a cylindrical ceramic heater of 5 mm in diameter. Typically, 0.02 g of catalyst powders were mixed with absolute ethanol to prepare a paste, and the paste was coated on the surface of heating tube; and then, it was heated in an oven at 110 ^oC for 24 h and heated at 450 °C for 1 h in air to form a coating. In order to accurately control the thickness, the same procedure was repeated. The obtained sensor was set in a quartz tube of 12-mm (i.d.) through which an air at atmospheric pressure flows at a constant rate. A certain volume pulse of CO was injected into the flow of air. The sample gas can flow only through the outside of the ceramic heater because this ceramic tube is solid. The temperature of the sensor was controlled using a digital temperature controller. The CL intensity was measured by a photon-counting method with a BPCL ultraweak chemiluminescence analyzer (BPCL, Chemiluminescence analyzer made by Biophysics Institute of the Chinese Academy of Science). In the experiment, the optical filter with the wavelength of 610 nm was used. Before each test, the catalyst sensor was heated at 450 °C for 1 h in air to avoid the influence of previous absorbates.

2.5. Catalytic Combustion of CH_4

The reaction of methane combustion was carried out in a conventional flow system under atmospheric pressure. 1 mL of the sample (20-40 mesh) was loaded in a quartz reactor (i.d. = 10 mm), packed with quartz beads on both top and bottom of the catalyst bed. A mixture gas of methane (3 vol.%) and air (97 vol.%) was fed into the catalyst bed at a gas hourly space velocity (GHSV) of 60, 000 h^{-1}. The inlet and outlet gas compositions were analyzed by on-line gas chromatography, using a packed column of carbon molecular sieves and a thermal conductivity detector (TCD). Before each run, the catalyst was flushed with air at 450 ^oC for 0.5 h in order to remove the previous absorbates from the catalyst surface, and then cooled to 30 ^oC. Here, the temperatures at 10% and 90% conversions of methane were designated as T_{10} and T_{90}, respectively, which were used to compare activities of the catalysts.

3. RESULTS AND DISCUSSION

3.1. Morphologies, Crystal Phases and Textures of ZrO_2 Samples

Fig. (**1**) presents the SEM images of ZrO_2 samples after being calcined at 550 ^oC for 5 h. A network of nanorods (NRs) was prepared using this template route, and the nanorods have the diameters in the range of 50-100 nm (Fig. **1a**); but the uniform nanoparticles (NPs) of 50 nm in size were obtained by a hydrothermal method (Fig. **1b**). It is clear that the preparation method has a significant influence on the morphology of the sample. It is well known that there are a plenty of functional groups (e.g., amines, amides and carboxylic) on the surface of this bio-membranes template [29]. Zirconium ions can be easily chelated or adsorbed onto the template surface, as a result, the coating of zirconium on the template can form. While the hybrid gel formed, the morphology of biomemberane could also be transcribed into the zirconium hydroxide gel. The framework of the hybrid gel is further solidified after being aged and dried. After calcination, the formed zirconia sample maintained the network morphology. The morphology templating process is similar to our previous study [30], in which we have prepared alumina nanorods use CMC (carboxymethyl cellulose) network. In this work, we have not obtained ZrO_2 nanotubes as reported by Qi *et al*. [10]. The reason is still not clear. In our experiment, $ZrOCl_2$ was used as the Zr source, while Qi *et al*. use zirconium propoxide was used as the Zr source [10]. We could believe that this may be related to the different Zr source.

We further investigated the stabilities of these samples. As shown in Fig. (**1c**, **d**), after being calcined at 800 ^oC for 24 h in air, a significant constriction can be observed for the nanorod network; but the nanoparticles have grown and/or agglomerated into the large particles of 0.5-1 μm in sizes. Fig. (**2**) shows XRD patterns of ZrO_2 samples. The as-synthesized sample by template mainly consists of tetragonal phase containing small amounts of monocilinic phase; after calcinations at 800 ^oC, the amount of monocilinic phase increased while that of tetragonal phase decreased; as a result,

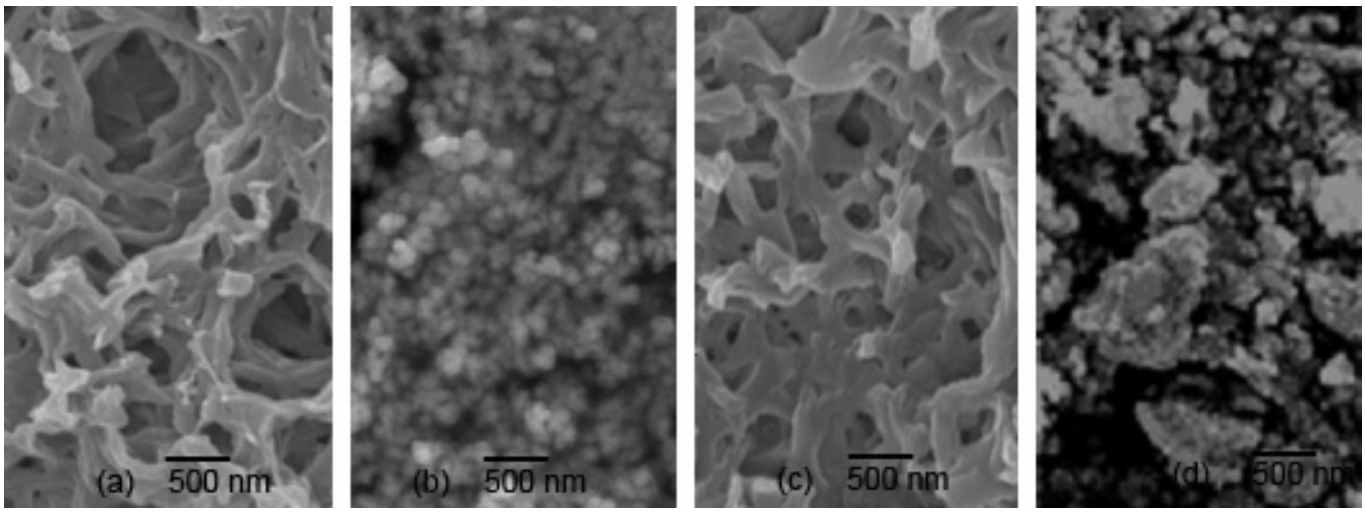

Fig. (1). SEM images of ZrO_2 samples: (**a**,**b**) NRs and NPs, Nanorod network and nanoparticles before calcination at 800 °C, respectively; (**c**,**d**) NRs800 and NPs800, Nanorod network and nanoparticles after calcination at 800 °C for 24 h, respectively.

the calcined sample consisted of more monocilinic and less tetragonal phases. By the hydrothermal method, the as-synthesized sample mainly consisted of monocilinic phase with a little tetragonal phase. After calcinations at 800 °C, the diffraction peaks of the sample become sharper, indicating that the crystals grew significantly. Calculated by Scherrer equation, the crystal size of the nanorod sample increased from 15.8 to 20.5 nm; but the crystal size of the nanoparticle sample significantly increased from 10.6 to 50.8 nm. The above results indicate that a tetragonal-monoclinic phase transformation occurred, leading to the formation of more monoclinic phase. It has been documented that the hydrated $Zr(OH)_2$ can crystallize into a tetragonal ZrO_2 upon annealing and the tetragonal-to-monoclinic phase transformation can occur at various temperatures for nanocrystals [31].

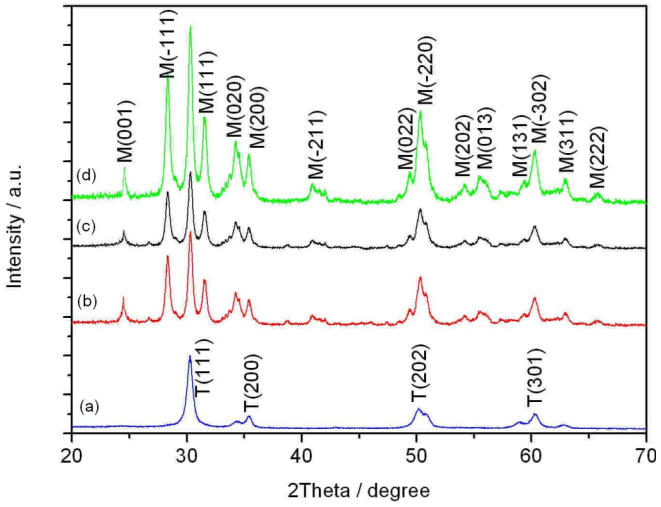

Fig. (2). XRD patterns of ZrO_2 samples: (**a**) NRs, (**b**) NPs, (**c**) NRs800, (**d**) NPs800.

The textural properties of the samples were investigated further, as shown in Table **1** and Fig. (**3**). The rodlike sample had the larger pore volume (0.42 cm^3 g^{-1}) than that (0.24 cm^3 g^{-1}) of the nanoparticles. Notably, after being calcined at 800 °C for 24 h, although a significant volume contraction (about 52 vol.%) of ZrO_2 nanorod network occurred, the sample had a large pore volume (0.20 cm^3 g^{-1}); but the nanoparticle sample had much small pore volume (0.05 cm^3 g^{-1}), indicating that the nanoparticle sample had sintered more severely than the rodlike network during the calcination process. As a result, the BET area of nanoparticle sample decreased about 54.8% (55.8 *vs* 25.2 m^2 g^{-1}); however, the surface area of the rodlike network decreased about 19.5% (56.7 *vs* 45.7 m^2 g^{-1}). Horiuchi *et al*. [32] have reported that the nucleation of α-Al_2O_3 phase first occurred at the contacting neck between the particles. Because the contacting points between the particles are considered as the nucleating and/or sintering sites, the decrease of contacting chance would suppress the phase transformation and the particle sintering. Their differences in thermal stability may be related to their different morphologies. It is well known that the nanoparticles are easy to pack closely, which means that there are more contacting points among the particles. Therefore, the ZrO_2 nanoparticles would sinter severely under the high-temperature calcination. As shown in Fig. (**3**), however, the rodlike network with a loose structure has advanced pores, meaning that the contacting points among the particles are less; and the sintering of the network of nanorods was refrained to some extent. As a result, the rodlike network has a higher surface area. It could be assumed that the advanced pore structure of network has relieved the sintering of particles effectively. Barry *et al*. [33] have also prepared fibrous Al_2O_3 with a high surface area at high temperature and they ascribed the high ability resistant to sintering to the crude structure and fiberform morphology for Al_2O_3 particles. According to the research of Ishikawa *et al*. [34], the sintering of Al_2O_3 proceeds simultaneously with phase transition from a metastable phase to α-Al_2O_3 at the contacting neck between the particles.

3.2. Cataluminescence (CL) Properties of CO Oxidation Over ZrO_2 Samples

Typically, we determined CL intensities of CO oxidation over ZrO_2 nanorod network at different test temperature (*T*). Observed from Fig. (**4**), the CL intensities increased from 1.5×10^3 to 1.5×10^4 a.u. while the temperature increased from 200 to 400 °C. It is clear that the test temperature has a significant influence on CL intensity. This is because CO conversion increased with the temperature. More CO molecules

Table 1. Surface Areas, Particle Sizes and Crystal Sizes of ZrO_2 Samples

Sample	[b] SA (m^2 g^{-1})	[c] V_p (cm^3 g^{-1})	[d] d_p (nm)	[e] $D_{t(111)}$
[a] NRs	56.7	0.42	32.2	15.8
[a] NRs800	45.7	0.20	25.8	20.5
[a] NPs	55.8	0.24	11.5	10.6
[a] NPs800	25.2	0.05	38.5	50.8

[a] NRs and NRs800, Nanorod network before and after calcination at 800 °C, respectively; NPs and NPs800, Nanorod network before and after calcination at 800 °C, respectively; [b] Surface area calculated by the BET method, [c] Pore volume calculated by the BJH method, [d] Average pore size, [e] Crystal size calculated by Scherrer equation.

were oxidized into CO_2 molecules at high temperatures. It is important for CL determination to maintain a constant test temperature. Fig. (**5**) gives the typical CL spectra of CO over ZrO_2 samples at 400 °C. Our experiments showed that while heating the catalysts in the absence of CO or heating the flowing mixed gases of CO and air, no emission of thermoluminescence can be observed. This confirms that the luminescence signal results from the catalytic oxidation process of CO by the catalyst. It could be observed that CL intensity at maximum (1.52×10^4 a.u.) of NPs is higher than that (1.15×10^4 a.u.) of NRs. Note that the thermal stability of a catalyst is an important factor for the practice applications. Nevertheless, CL intensity at maximum (0.75×10^4 a.u.) of NRs800 was higher than that (0.61×10^4 a.u.) of NPs800. This result may be closely related to their BET areas. Moreover, the porous networks with a higher BET area may favor for the good mass transport and the accessibility of gases to solid, compared with the less porous sample with a low BET area. As far as CL mechanism is concerned, Breysse *et al*. [35] have proposed a mechanism of recombination radiation of ThO_2. CO is chemisorbed on the surface of ThO_2, and combined with surface hole to form the CO^+ ion; O_2 is dissociated and chemisorbed on the surface of ThO_2, and combined with surface electron to form the O^- ion. This means that the chemisorbed CO forms a positively ionized surface state (the surface donor state) accompanied by the localized hole; and the chemisorbed oxygen forms a negatively ionized surface-state (the surface acceptor state) accompanied by the localized electron. Surface reaction between these chemisorbed species will occur to form the chemisorbed CO_2. The chemisorbed CO_2 accompanied by the localized electron and hole is a chemisorption surface state bound to an exciton. CO_2 desorption is accompanied by annihilation of the exciton, and luminescence is emitted by recombination of electron and hole. In consideration of their similar crystalline phases, the large BET area of NPs800 could favor for the adsorption of the reacting gases and form more positive CO^+ surface negative O^-, which needs further research. As a result, the network of nanorods had a higher CL intensity, and could potentially be used to fabricate a stable CL sensor.

3.3. Combustion Activities of CH_4 Over ZrO_2 Samples

It is well known that at low conversions of methane, methane combustion is controlled mainly by surface catalytic reaction; at high conversions of methane, the oxidation of methane usually includes surface reaction and free radical reaction. The free radical reactions are more dependent on mass transfer than on the surface reaction. Before the gases

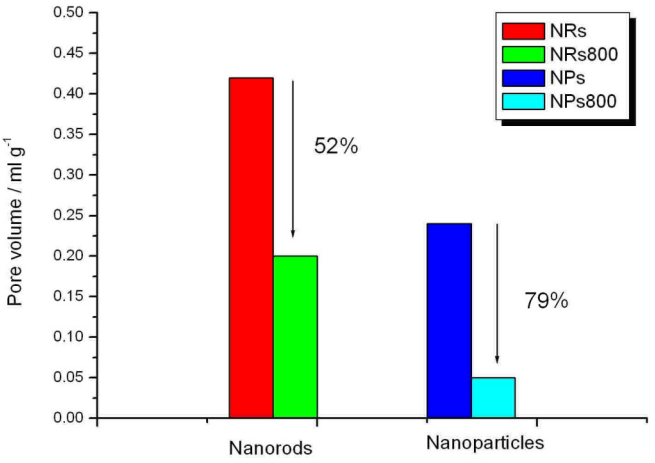

Fig. (3). Pore volumes of ZrO_2 samples before and after calcination at 800 °C for 24 h.

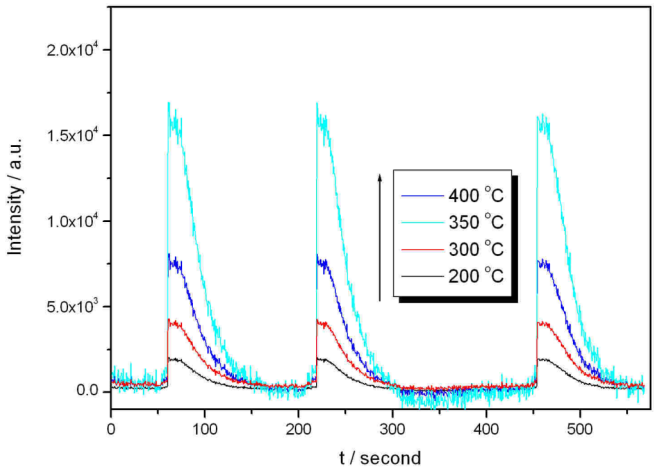

Fig. (4). CL intensities of CO oxidation over ZrO_2 nanorod network at different temperatures: F (Flowing rate of gas) = 200 mL min^{-1}; C (CO concentration) = 200 μg mL^{-1}, λ_{filter} (Wave length of filter) = 610 nm.

reacted on the solid surface, the gas diffusion from bulk gases to the solid surface occurred. Because the surface reaction is relative fast, the influence of mass transfer from gas bulk to the catalyst surface on the reaction should not be ignored. The balance between surface reaction and mass transfer may be affected by various factors, e.g., intrinsic activity, particle sizes, porosity and concentration of catalyst, etc. The large surface area of the catalyst is beneficial to mass transfer, since the large surface area and advanced pores may favor for the adsorption of more gases on the

solid surface. The combustion activities of methane over ZrO_2 samples were also investigated, as shown in Fig. (**6**). The ignition temperature (T_{10}) and the complete combustion temperature (T_{90}) of ZrO_2 NRs800 are ca. 680 and 770°C, which are 20 and 40 °C lower than those (T_{10} = 700 °C, T_{90} = 810 °C) of NPs800, respectively. The nanorod network shows a higher activity than the latter. It seems that the texture properties have a more significant influence on the catalyst activity at high conversions of methane than at low conversions. The activity difference could be ascribed to their different surface area and advanced pores, which favor for the process of mass-transformation.

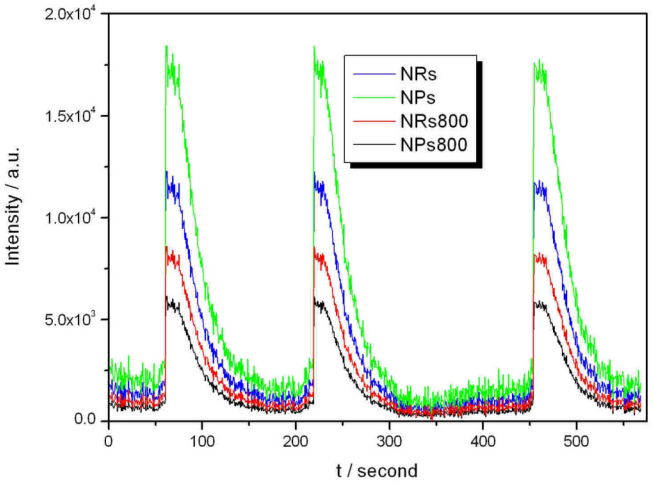

Fig. (5). The CL spectra of CO over (**a**) ZrO_2 nanorod network and (**b**) ZrO_2 nanoparticles: T = 400 °C, F = 200 mL min^{-1}, λ_{filter}= 610 nm, C = 200 μg mL^{-1}.

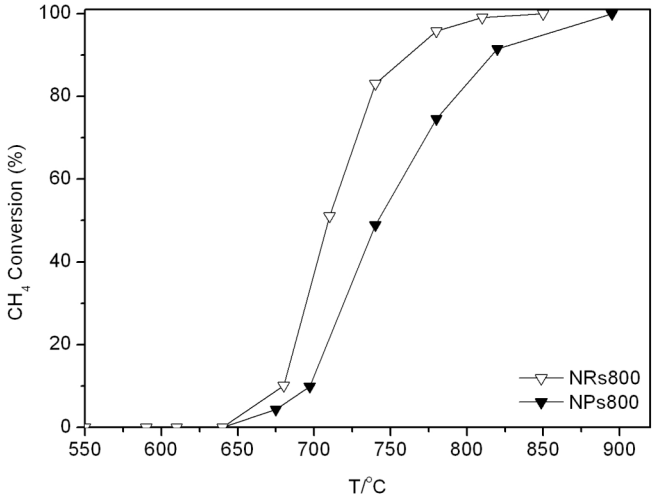

Fig. (6). Light-off curves of methane combustion over ZrO_2 nanorod network and particles: GHSV (gas hourly space velocity) = 60, 000 h^{-1}, 3 vol.% CH_4, 97 vol.% air.

4. CONCLUSION

A bio-membrane has been successfully applied for synthesis of ZrO_2 with a porous network of ZrO_2 nanorods. These results suggest that the biomimetic synthesis can be used to synthesize advanced-structure materials, which is not easy to obtain by the synthetic templates. After calcination at 800 °C, the porous network of ZrO_2 nanorod network has a high surface area and advanced pores; and they had a high CL intensity of CO oxidation and a high combustion activity of CH_4.

ACKNOWLEDGEMENTS

This work is financially supported by Michigan Tech Faculty Startup Fund (N4901928249), National Basic Research Program of China (Grant 2007CB613303) and Chinese National Science Foundation (Grants 20433010 and 20571047).

REFERENCES

[1] Hu, J.T.; Ouyang, M.; Yang, P.D.; Lieber, C.M. Controlled growth and electrical properties of heterojunctions of carbon nanotubes and silicon nanowires. *Nature,* **1999**, *399*, 48-51.

[2] Xu, D.; Xu, Y.; Chen, D.; Guo, G.; Gui, L.; Tang, Y. Preparation of CdS single-crystal nanowires by electrochemically induced deposition. *Adv. Mater.,* **2000**, *12* (7), 520-22.

[3] Heath, J.R.; Kuekes, P.J.; Snyder, G.; Williams, R.S. A defect-tolerant computer architecture: opportunities for nanotechnology. *Science*, **1998**, *280*, 1716-21.

[4] Zhou, K.; Wang, X.; Sun, X.; Peng, Q.; Li, Y. Enhanced catalytic activity of ceria nanorods from well-defined reactive crystal planes. *J. Catal.*, **2005**, *229*, 206-12.

[5] Zhao, N.; Pan, D.; Nie, W.; Ji, X. Two-phase synthesis of shape-controlled colloidal zirconia nanocrystals and their characterization. *J. Am. Chem. Soc*., **2006**, *128*, 10118-24.

[6] Chuach, G.K.; Jaenicke, S.; Cheong, S.A.; Chan, K.S. The influence of preparation conditions on the surface area of zirconia. *Appl. Catal. A*, **1996**, *145*, 267-84.

[7] Minh, N.Q. Ceramic fuel-cells. *J. Am. Ceram. Soc.,* **1993**, *76* (3), 563-88.

[8] Crepaldi, E.L.; de, G.J.; Soler-Illia, A.A.; Grosso, D.; Albouy, P.-A.; Sanchez, C. Design and post-functionalisation of ordered mesoporous zirconia thin films. *Chem. Commun.*, **2001**, *23*, 1582-83.

[9] Tsuchiya, H.; Macak, J.M.; Taveira, L.; Schmuki, P. Fabrication and characterization of smooth high aspect ratio zirconia nanotubes. *Chem. Phys Lett.*, **2005**, *410*, 188-91.

[10] Yang, D.; Qi, L.; Ma, J. Hierarchically ordered networks comprising crystalline ZrO_2 tubes through sol-gel mineralization of eggshell membranes. *J. Mater. Chem.*, **2003**, *13*, 1119-23.

[11] Bao, J.C.; Xu, D. P.; Zhou, Q. F.; Xu, Z. An array of concentric composite nanostructure of metal nanowires encapsulated in zirconia nanotubes: Preparation, characterization, and magnetic properties. *Chem. Mater.*, **2002**, *14*, 4709-13.

[12] Bao, J.; Tie, C.; Xu, Z.; Ma, Q.; Hong, J.; Sang, H.; Sheng, D. An array of concentric composite nanostructures of zirconia nanotubules/cobalt nanowires: preparation and magnetic properties. *Adv. Mater.*, **2002**, *14*, 44-7.

[13] Rao, C.N.R.; Satishkumar, B.C.; Govindaraj, A. Zirconia nanotubes. *Chem. Commun*., **1997**, *16*, 1581-82.

[14] Shin, H.; Jeong, D.-K.; Lee, J.; Sung, M.M.; Kim, J. Formation of TiO_2 and ZrO_2 nanotubes using atomic layer deposition with ultra-precise control of the wall thickness. *Adv. Mater.*, **2004**, *16*, 1197-1200.

[15] Tsuchiya, H.; Schmuki, P. Thick self-organized porous zirconium oxide formed in H_2SO_4/NH_4F electrolytes. *Electrochem. Commun.*, **2004**, *6*, 1131-4.

[16] Noh, H.-J.; Seo, D.-S.; Kim, H.; Lee, J.-K. Synthesis and crystallization of anisotropic shaped ZrO_2 nanocrystalline powders by hydrothennal process. *Mater. Lett.*, **2003**, *57*, 2425-31.

[17] Li, L.; Wang, W. Synthesis and characterization of monoclinic ZrO_2 nanorods by a novel and simple precursor thermal decomposition approach. *Solid State Commun*., **2003**, *127*, 639-43.

[18] Grover, V.; Shukla, R.; Tyagi, A.K. Facile synthesis of ZrO_2 powders: control of morphology. *Scripta Materialia*, **2007**, *57*, 699-702.

[19] Wang, Z.; Tao, D.; Guo, G.; Jin, S.; Wei, F.; Qian, W.; Hong, S. Synthesis of dispersed ZrO_2 nano-laminae composed of ZrO_2 nanocrystals. *J. Mater. Lett.*, **2006**, *60*, 3104-8.

[20] Mann, S. The chemistry of form. *Angew. Chem., Int. Ed.*, **2000**, *39*, 3393-406.

[21] Ogasawara, W.; Shenton, W.; Davis, S.A.; Mann, S. Template mineralization of ordered macroporous chitin-silica composites us-

ing a cuttlebone-derived organic matrix. *Chem. Mater.*, **2000**, *12*, 2835-7.

[22] Meldrum, F.C.; Seshadri, R. Porous gold structures through templating by echinoid skeletal plates. *Chem. Commun.*, **2000**, *22*, 29-30.

[23] Seshadri, R.; Meldrum, F.C. Bioskeletons as templates for ordered, macroporous structures. *Adv. Mater.*, **2000**, *12*, 1149-52.

[24] Davis, S.A.; Burkett, S.L.; Mendelson, N.H.; Mann, S. Bacterial templating of ordered macrostructures in silica and silica-surfactant mesophases. *Nature*, **1997**, *385*, 420-3.

[25] Zhang, B.; Davis, S.A.; Mendelson, N.H.; Mann, S. Bacterial templating of zeolite fibres with hierarchical structure. *Chem. Commun.*, **2000**, *1*, 781-2.

[26] Shin, Y.; Liu, J.; Chang, J.H.; Nie, Z.; Exarhos, G. J. Hierarchically ordered ceramics through surfactant-templated sol-gel mineralization of biological cellular structures. *Adv. Mater*., **2001**, *13*, 728-32.

[27] Dong, A.; Wang, Y.; Tang, Y.; Ren, N.; Zhang, Y.; Yue, Y.; Gao, Z. Zeolitic tissue through wood cell templating. *Adv. Mater*., **2002**, *14*, 926-9.

[28] Yang, D.; Qi, L.; Ma, J. Eggshell membrane templating of hierarchically ordered macroporous networks composed of TiO_2 tubes. *Adv. Mater.*, **2002**, *14*, 1543-6.

[29] Ishikawa, S.; Suyama, K.; Arihara, K.; Itoh, M. Uptake and recovery of gold ions from electroplating wastes using eggshell membrane. *Bioresour. Technol.,* **2002**, *81*, 201-6.

[30] Teng, F.; Wang, J.; Tian, Z.; Wang, Z.; Xiong, G.; Xu, Z.; Xu, Y.; Lin, L. Morphology transcription process from CMC micelles to inorganogel and its effect on the properties of alumina particle. *Mater. Sci. Eng. B*, **2005**, *116*, 215-20.

[31] Shukla, S.; Seal, S.; Vij, R.; Bandyopadhyay, S.; Rahman, Z. Effect of nanocrystallite morphology on the metastable tetragonal phase stabilization in zirconia. *Nano Lett.*, **2002**, *2*, 989-93.

[32] Horiuchi, T.; Osaki, T.; Sugiyama, T.; Mori, T. Maintenance of large surface area of alumina heated at elevated temperatures above 1300 degrees C by preparing silica-containing pseudoboehmite aerogel. *J. Non-cryst. Solids*, **2001**, *291*, 187-98.

[33] Zhu, H.; Riches, J. D.; Barry, J.C. Gamma-alumina nanofibers prepared from aluminum hydrate with poly(ethylene oxide) surfactant. *Chem. Mater.*, **2002**, *14*, 2086-93.

[34] Ishikawa, T.; Ohashi, R.; Nakabayashi, H.; Ueno, A.; Furuta, A. Thermally stabilized transitional alumina prepared by fume pyrolysis of boehmite sols. *J. Catal.*, **1992**, *134*, 87-97.

[35] Breysse, M.; Claudel, B.; Faure, L.; Guenin, M.; Williams, R.J.J.; Wolkenstein, T.J. Chemiluminescence during catalysis of carbon-monoxide oxidation on a thoria surface. *J. Catal.*, **1976**, *45*, 137-44.

Received: November 7, 2008 Revised: February 2, 2009 Accepted: March 26, 2009